Published in final edited form as:
Sci Signal. ; 4(157): ra4. doi:10.1126/scisignal.2001225.

Genome-Wide RNAi Screen Reveals Disease-Associated Genes That Are Common to Hedgehog and Wnt Signaling

Leni S. Jacob[1], **Xiaofeng Wu**[1], **Michael E. Dodge**[1], **Chih-Wei Fan**[1], **Ozlem Kulak**[1], **Baozhi Chen**[1], **Wei Tang**[1,*], **Baolin Wang**[2,3], **James F. Amatruda**[4,5], and **Lawrence Lum**[1,†]

[1]Department of Cell Biology, University of Texas Southwestern Medical Center, Dallas, TX 75390, USA

[2]Department of Cell and Developmental Biology, Weill Cornell Medical College, New York, NY 10065, USA

[3]Department of Genetic Medicine, Weill Cornell Medical College, New York, NY 10065, USA

[4]Department of Pediatrics, University of Texas Southwestern Medical Center, Dallas, TX 75390, USA

[5]Department of Molecular Biology, University of Texas Southwestern Medical Center, Dallas, TX 75390, USA

Abstract

The Hedgehog (Hh) and Wnt signal transduction pathways are master regulators of embryogenesis and tissue renewal and represent anticancer therapeutic targets. Using genome-wide RNA interference screening in murine cultured cells, we established previously unknown associations between these signaling pathways and genes linked to developmental malformations, diseases of premature tissue degeneration, and cancer. We identified functions in both pathways for the multitasking kinase Stk11 (also known as Lkb1), a tumor suppressor implicated in lung and cervical cancers. We found that Stk11 loss resulted in disassembly of the primary cilium, a cellular organizing center for Hh pathway components, thus dampening Hh signaling. Loss of Stk11 also induced aberrant signaling through the Wnt pathway. Chemicals that targeted the Wnt acyltransferase Porcupine or that restored primary cilia length by inhibiting the tubulin deacetylase HDAC6 (histone deacetylase 6) countered deviant pathway activities driven by Stk11 loss. Our study demonstrates that Stk11 is a critical mediator in both the Hh and the Wnt pathways, and our approach provides a platform to support the development of targeted therapeutic strategies.

INTRODUCTION

Studies spanning nearly a half-century aimed at elucidating the underlying mechanisms of embryonic development in metazoans have yielded a handful of secreted intercellular signaling molecules that determine cell fate. These include members of the Hedgehog (Hh) and Wnt families, which additionally maintain homeostatic tissue renewal in adult animals and frequently contribute to degenerative disease and cancer (1, 2). Despite some successes

†To whom correspondence should be addressed. lawrence.lum@UTSouthwestern.edu.
*Present address: BioDuro Co. Ltd., No. 29 Building, Life Science Park Road, Changping District, 102206 Beijing, People's Republic of China.

Author contributions: L.S.J., X.W., M.E.D., C.-W.F., O.K., B.C., and W.T. performed all the experiments. L.S.J., X.W., M.E.D., C.-W.F., O.K., J.F.A., and L.L. designed the experiments and analyzed the data. B.W. provided reagents. L.S.J. and L.L. wrote the paper.

Competing interests: L.L., B.C., W.T., and M.E.D. are listed as inventors in a pending patent application associated with the IWR/IWP compounds described in this study.

in pharmacologically influencing the Hh and Wnt pathways (3, 4), the effective deployment of small molecules that target these pathways is limited by our understanding of pathway complicity in disease etiology.

The coordinated action of several well-defined pathway components transduces signals from Hh or Wnt into cellular responses specific to each ligand (5, 6). Essential to the fidelity of these signaling processes is the dynamic redistribution of pathway components to subcellular compartments that function as signaling relay points upon pathway stimulation. In the Hh pathway, the antenna-like primary cilium functions as an assembly area for pathway regulators (7) and contains the molecular machinery that mediates constitutive proteolytic processing of Gli transcriptional activators into repressor molecules (8–10). Activation of Hh-mediated response first entails engagement of Hh with the Dally-like protein (Dlp), Cell adhesion molecule–related/down-regulated by oncogenes (Cdo), and Patched (Ptch) receptors (5). In response to Ptchmediated reception of Hh, the Smoothened (Smo) transmembrane effector accumulates in the primary cilium, disengages Gli protein processing, and induces Gli-dependent transcription of target genes (11). Wnt is a ligand that stimulates multiple downstream pathways, those involving activation of the transcriptional coactivator β-catenin and those independent of the β-catenin effector (so-called canonical or noncanonical Wnt pathway responses, respectively) (2). Common to the known Wnt pathways is the activation of the Dishevelled (Dvl) signaling molecule, which typically entails its phosphorylation and redistribution from the cytoplasm to membrane-bound receptors in response to Wnt stimulation (2).

We performed a genome-wide RNA interference (RNAi) screen in cultured mouse cells to identify genes involved in both Hh and Wnt signaling. From this gene set, we discovered unanticipated associations between these pathways and genes previously linked to disease. We demonstrated that the tumor suppressor serine-threonine kinase and cell polarity regulator Stk11 (also known as Lkb1) functions as a component of both Hh and Wnt pathways. We found that Stk11 influenced the response to Hh by controlling the length of the primary cilium and Wnt responses by gating the abundance of phosphorylated Dvl protein. We formulated chemically based approaches to impede the altered cell signaling in cancerous cells lacking Stk11, which suggests that our screening strategy may be useful in defining molecular targets for therapeutic approaches for other diseases associated with multifunctional genes.

RESULTS

A genome-wide RNAi screen identifies disease-associated genes with potential roles in Hh and Wnt pathway response

To identify previously unknown Hh pathway components, we performed two parallel genome-wide RNAi screens in cultured cells by transiently introducing gene-specific small interfering RNA (siRNA) pools (four non-redundant siRNAs) from two mouse siRNA libraries into 3T3-ShhFL cells (Fig. 1A; fig. S1, A to F; and tables S1 and S2). The 3T3-ShhFL cells enable monitoring of Sonic hedgehog (Shh)–induced transcriptional response in a cell-autonomous manner with a well-established Hh pathway reporter (the GliBS reporter) (12). Because these cells produce Shh, targeting of genes encoding proteins involved in either Shh production or downstream signaling can reduce reporter activity. With this system, we screened a combined total of 39,000 siRNA pools, with ~15,700 of these mutually targeting the same genes with mostly nonoverlapping siRNA sequences (13) (Fig. 1A). Focusing on positive pathway regulators (siRNAs that reduced reporter activity greater than two SDs from the mean signal), we identified 535 genes of interest (tables S3 and S4). Recovery of known Hh pathway components such as Smo, the seven-transmembrane pathway effector, and components of the primary cilium was improved with the use of both

siRNA libraries, suggesting an advantage in using multiple siRNA libraries in RNAi-based screening strategies (Fig. 1B). We were also intrigued by the sparseness of overlapping genes identified from the initial parallel screening of two siRNA libraries and further interrogated this phenomenon with additional RNAi-based studies using conditions that minimize inherent noise associated with high-throughput screening platforms (fig. S1, G and H). These additional studies revealed that the integration of RNAi-derived data sets is limited by the effectiveness of the siRNA design and current high-throughput screening formats and showed the need to screen multiple siRNA libraries to reduce false-negative discovery rates.

We retested the siRNAs against the 535 genes of interest in ShhLightII cells stimulated with exogenous Shh to enrich for genes that act downstream of Shh protein production (Fig. 1C). ShhLightII cells are NIH 3T3 cells that do not endogenously produce Shh and are stably transfected with the GliBS reporter. We counterscreened the resulting hits against the Wnt/ □catenin pathway in NIH 3T3 cells with a Wnt-responsive luciferase reporter [SuperTopFlash (STF)] (Fig. 1, C and D). Genes when targeted with siRNAs that decreased activities of both pathways may influence cell viability and were not considered for further testing. We cross-referenced the remaining genes with the OMIM (Online Mendelian Inheritance in Man) database to identify previously unknown associations between diseases and the Hh and Wnt pathways (Fig. 1, C and D).

We confirmed the specificity of siRNA pools targeting the disease-associated genes by evaluating the ability of individual siRNAs from the pool to recapitulate the original observation (fig. S2 and table S5). Genes already validated by identification from two siRNAs pools were not retested. Using a minimum threshold of three distinct siRNAs inducing a shared phenotypic outcome as the criteria for high-confidence genes with minimal influence from RNAi off-targeting (14), we retained a total of 10 genes associated with either malformation, degenerative disease, or cancer (Table 1). The heparan sulfate proteoglycan glypican 1 (Gpc1) is a homolog of Dlp that functions as part of the receptor complex for Hh in *Drosophila* (15). Prkar1a, the regulatory subunit of protein kinase A (PKA), was previously identified as critical to Hh pathway response in a kinome-wide RNAi screen (14). We also identified two gene products linked to ciliopathies: retinaldehyde-binding protein 1 (Rlbp1) and intraflagellar transport 57 (Ift57) (16, 17). With the exception of Smo and Gli2, the Hh-related functions of the remaining genes [the serine-threonine kinase Stk22b; diacyl-glycerol kinase □(*Dgkq*); and the achalasia, adrenocortical insufficiency, alacrima syndrome (*Aaas*) gene] are unknown. The Stk11 tumor suppressor controls microtubule dynamics, metabolism, and cell polarity but has not been previously implicated in Hh-mediated signaling (18).

Prkar1a and Stk11 control the abundance of the Gli3 transcriptional repressor

Among the genes identified as potential Hh pathway regulators, Prkar1a and Stk11 are both recognized as tumor suppressors (Table 1). By analyzing the transcriptional response to Shh in mouse embryonic fibroblasts (MEFs) null for *PRKAR1a* or *STK11*, we confirmed that loss of either of these two molecules decreased Hh pathway response (Fig. 2, A to C). Whereas the requirement for Prkar1a in Hh-induced expression of *Ptch1* has been reported, its mechanism of action within the pathway has not been well interrogated. In accordance with the role of PKA in Gli processing, loss of Prkar1a results in an increase in the amount of Gli3 repressor (Gli3R), presumably as a result of unregulated PKA activity (19) (Fig. 2D). $STK11^{-/-}$ MEFs also exhibited increased Gli3R abundance relative to wild-type MEFs that cannot be accounted for by changes in the *Gli3* expression (Fig. 2E and fig. S3A). Unlike in the *PRKAR1A*-null cells, the production of Gli3R in *STK11*-null cells was reduced by Shh protein or a Smo agonist (SAG), suggesting that Smo function was intact (Fig. 2E). Pulse-chase analysis of the rate of Gli3R formation after addition of either SAG or

Hh-conditioned medium confirmed that the rate of Gli3R formation was increased by nearly threefold in *STK11*-null MEFs relative to that in wild-type MEFs (Fig. 2F and fig. S3B). Furthermore, in the presence of a proteasome inhibitor, which blocks Gli3R production, the stability of Gli3R does not appear to be increased in *STK11*-null MEFs when compared to that in wild-type MEFs. Thus, alteration of the Gli3R turnover rate does not appear to contribute to the accumulation of Gli3R observed in *STK11*-null MEFs (Fig. 2G).

Stk11 regulates primary cilia length

To further understand the mechanism underlying the Stk11-induced increase in the abundance of Gli3R, we examined the primary cilium, an organelle essential for proteolytic processing of Gli molecules into transcriptional repressors (7). The cilia in $STK11^{-/-}$ cells were on average one-half the length of their counterparts in wild-type cells, suggesting a defect in achieving the normal length of this organelle in $STK11^{-/-}$ cells (Fig. 3A and fig. S3C). Examination of cilia in $STK11^{-/-}$ cells by transmission electron microscopy confirmed the establishment of a basal body, the cellular anchor of cilia, and the ability of $STK11^{-/-}$ cells to elaborate rudimentary cilia (Fig. 3B). Because the dynamics of cilia formation and disassembly are influenced by the cell cycle, and $STK11^{-/-}$ MEFs double more rapidly than do wild-type MEFs (20) (fig. S3D), we analyzed the propensity of the wild-type and $STK11^{-/-}$ MEFs to exhibit growth arrest under conditions typically used to examine primary cilia (low serum, high cell density). Both cell lines achieved cell cycle arrest at confluency, suggesting that the differences in primary cilium length are not attributable to changes in the duration of cell cycle phases (Fig. 3C).

The tubulin deacetylase HDAC6 (histone deacetylase 6) promotes ciliary disassembly and thus influences cilia length (21). Addition of suberoylanilide hydroxamic acid (SAHA), an inhibitor of deacetylases including HDAC6 (22), increased cilia length in $STK11^{-/-}$ cells but not in wild-type cells, suggesting that $STK11^{-/-}$ cells undergo excessive cilia disassembly (Fig. 3, D and E). Consistent with this model, the HDAC6 inhibitor tubacin, but not the HDAC1 inhibitor MS-275, restored cilia length in $STK11^{-/-}$ cells (Fig. 3E and fig. S3E). The extension of primary cilia in SAHA-treated cells also correlated with restoration of Gli3R to an amount similar to that in wild-type cells (Fig. 3F). Concomitantly, SAHA increased the abundance of acetylated tubulin, which is decreased in $STK11^{-/-}$ cells, compared to wild-type cells (Fig. 3F). Considering that Gli proteins must cycle through the primary cilium to acquire PKA-dependent phosphorylation before proteolytic processing in the cytoplasm (23–25), the increased abundance of the GliR molecules may be due to decreased transit time of full-length Gli molecules in the shortened cilia. However, we cannot rule out the contribution of other Stk11-dependent mechanisms that may directly influence Gli processing.

We also examined in $STK11^{-/-}$ cells the ability of Hh pathway components to accumulate in the primary cilium in response to Shh (26, 27). Consistent with the ability of Hh and SAG to block Gli3 processing (Fig. 2E), the translocation of Smo into the cilium and accumulation of Gli2 protein at the tip of the cilium in response to Shh appeared normal in the $STK11^{-/-}$cells (fig. S4, A and B). Thus, the excessive accumulation of Gli3R in $STK11^{-/-}$ cells is not likely due to altered subcellular localization of Smo or Gli proteins. We also confirmed, using a membrane-associated protein marker (Smo), that cilia length is decreased in $STK11^{-/-}$ cells (fig. S4C).

Loss of Stk11 induces a gain of Dvl protein function

We also identified Stk11 as a suppressor of Wnt-mediated responses (Fig. 1D). Examination of biochemical changes associated with Wnt/ □catenin pathway activity in $STK11^{-/-}$ MEFs revealed that the amount of phosphorylated Dvl2 was increased compared to that in wild-

type MEFs (Fig. 4A and fig. S5A). This phosphorylation was not sensitive to HDAC6 inhibitors, suggesting that in MEFs, acetylated tubulin abundance does not affect Dvl protein phosphorylation (fig. S5B). Phosphorylation of Dvl2 by casein kinase 1 (CK1) family members at consensus CK1 phosphorylation sites contributes to both β-catenin–dependent and noncanonical Wnt signal transduction (28). We interrogated altered pathway activity with a synthetic Wnt pathway inhibitor that targets the pathway at the level of Wnt production [inhibitor of Wnt production (IWP), an inhibitor of the acyltransferase Porcupine] (29) (Fig. 4B). The IWP compound restored the ratio of phosphorylated to unphosphorylated Dvl proteins in *STK11*$^{-/-}$ MEFs to that observed in wild-type MEFs, suggesting that the increased Dvl activity is dependent on production of endogenous Wnt protein (Fig. 4C and fig. S5C). Whereas specificity studies associated with the IWP compounds have been previously described (29), we provide here additional support for the mode of action attributed to these compounds (fig. S5, D and E). Consistent with the ligand-dependent activity of Dvl in *STK11*$^{-/-}$MEFs, inhibition of CK1, a kinase essential to ligand-mediated Dvl activity (28), reduced Dvl phosphorylation (Fig. 4D), whereas an inhibitor of PKA had little effect on Dvl phosphorylation (fig. S5F).

Dvl proteins function as cytoplasmic routers that can transduce both β-catenin–dependent and –independent Wnt-mediated responses (30). RNAi targeting of Dvl2 reduced the rate of growth in *STK11*$^{-/-}$ MEFs, suggesting that Dvl2 plays a key role in promoting aberrant cell proliferation (Fig. 4E). In response to Wnt, Dvl adopts a diffuse cytoplasmic distribution that contrasts with its localization to punctate structures in the absence of Wnt (31) (fig. S6). We found that there was abundant diffusely localized Dvl2 [fused to green fluorescent protein (GFP)] in *STK11*$^{-/-}$ MEFs even in the absence of added Wnt, and this contrasted with the distribution of a GFP-tagged Axin1, a binding partner of Dvl (31), which retained its typical punctate cellular distribution (Fig. 4F). Although IWP restored ratios of phosphorylated to unphosphorylated Dvl2 in the *STK11*$^{-/-}$ cells to that observed in wild-type MEFs (Fig. 4C), it failed to restore punctate Dvl distribution (Fig. 4F). Together, these findings suggest that loss of Stk11 results in altered Dvl protein distribution that facilitates Wnt-dependent Dvl phosphorylation.

Knockdown of Stk11 in zebrafish embryos causes developmental defects

We investigated the role of Stk11 in vivo by analyzing zebrafish embryos treated with morpholino oligonucleotides (MOs) targeting Stk11. Consistent with reduced Hh signaling, the embryos had U-shaped somites when analyzed at 24 hours after fertilization (Fig. 5A). We also noted that some treated embryos exhibited shortened tails, a phenotype that may arise from altered noncanonical Wnt-mediated responses (32) (Fig. 5A and fig. S7). *Engrailed 1a* (*Eng1a*) expression, which is associated with Hh signaling (33), was also reduced in the Stk11 morphants in the midbrain-hindbrain boundary and muscle pioneers (Fig. 5B). We also noted little change in β-catenin–dependent Wnt signaling (*axin2* expression) in zebrafish from the same developmental stage, suggesting potential differences in Stk11-mediated regulation of Wnt/β-catenin signaling across species or between developing and adult tissues (Fig. 5C). Together, these data are consistent with a role for Stk11 in both Hh and Wnt signaling in vivo but do not rule out the possibility that other functions of Stk11, such as its activity in cell polarity, also contribute to the observed developmental defects.

Cancerous cells lacking Stk11 engage deviant Wnt-mediated responses

Whereas the Stk11-associated Peutz-Jeghers hereditary tumor syndrome is a relatively rare disease, sporadic cancers, such as those from the lung and cervix, frequently harbor mutations in *STK11* (34, 35). We investigated the relevance of Stk11 loss in Wnt signaling in a panel of cells derived from cervical carcinoma. Consistent with our findings in MEFs,

cervical carcinoma cell lines, previously described as lacking Stk11 (35), all exhibited enhanced Dvl2 phosphorylation relative to normal endometrium-derived cells (Endo cells) (Fig. 6A). A similar link between Stk11 status and Dvl phosphorylation was also present in cell lines derived from another Stk11-associated cancer, non–small cell lung cancer (NSCLC) (fig. S8A). Notably, cells from this cancer type lacking *STK11* generally exhibit poor ciliogenesis, a phenotype that can be partially rescued by reintroduction of Stk11 DNA (fig. S8, B and C).

Despite the observation that the *STK11*-null cervical carcinoma cell lines uniformly exhibited an increase in Dvl phosphorylation, only a subset is positive for c-Myc protein, which is encoded by a target gene of the Wnt/β-catenin pathway (Fig. 6A). For example, HeLa and SiHa cells both lack Stk11, but only in HeLa cells was c-Myc detected. This suggests that the outcome of *STK11* loss is context specific with respect to aberrant engagement of Wnt signaling.

We confirmed the role of Stk11 in controlling Wnt/β-catenin pathway activity in HeLa cells. Consistent with the presence of c-Myc in these cells, we observed increased activity of the STF reporter in HeLa cells relative to that in Endo and SiHa cells (Fig. 6B). This reporter activity was sensitive to the IWP compound that disrupts Wnt ligand production, as well as a chemical that inhibits Wnt/β-catenin pathway activity by stabilizing Axin, a negative regulator of β-catenin [the inhibitor of Wnt response (IWR)] (Fig. 6B). We also noted in HeLa, but not SiHa cells, the presence of Axin2 and phosphorylated LRP6, both hallmarks of Wnt/β-catenin pathway activity (fig. S9).

Introduction of Stk11 into HeLa cells reduced the Wnt-mediated transcriptional response (Fig. 6C), partially restored the punctate distribution of Dvl2 (Fig. 6D) (Axin1 distribution shown in fig. S10), and promoted the appearance of nonphosphorylated Dvl2 (Fig. 6E). Expression of a kinase-dead (KD) form of Stk11 did not result in an increase in the abundance of unphosphorylated Dvl2, suggesting that kinase activity of Stk11 is essential to its ability to restrain Dvl activity (Fig. 6E). These observations, together with the ability of Stk11 to reduce cell growth (either by stalling proliferation or by inducing cell death) in HeLa cells (Fig. 6F), support a role for Stk11 in controlling cell growth or viability by influencing Wnt/β-catenin pathway activity. This cell growth regulation is not likely to involve Hh signaling, given that HeLa cells rarely form primary cilia (36). Engagement of Dvl as a consequence of Stk11 loss in cancerous cells may thus give rise to β-catenin–dependent or –independent Wnt-mediated responses, or both. Furthermore, the type of response is likely dictated by the expression pattern of Wnt family members and their receptors (37).

DISCUSSION

We used an RNAi screening approach in murine cultured cells to establish previously unknown relationships between two therapeutically relevant signal transduction pathways and genes of importance in diseases of cell growth, tissue degeneration, and malformation. We investigated the mechanism of action for Stk11 in both the Hh and the Wnt pathways and biochemically established a role for Prkar1a, the regulatory subunit of PKA, in governing GliR formation. The use of two readouts (Hh and Wnt pathway reporters) to elucidate cellular mechanisms of Stk11 function suggests that expanded data sets encompassing analysis of additional pathways would improve our capability to assign gene function to cellular processes.

Proteolytic processing of Gli proteins entails their cycling through the primary cilium to acquire PKA-dependent phosphorylation (23–25). However, this process has been difficult

to study, given that genetic approaches to disrupt intraciliary trafficking through targeted deletion of intraflagellar trafficking (IFT) complex components typically result in disruption of ciliogenesis as well as Gli processing (38–40). Our observations in *STK11*-null cells suggest that the length of the primary cilium controls the rate of Gli processing. The ability of the tubulin deacetylase inhibitors SAHA and tubacin to influence cilia length in *STK11*$^{-/-}$, but not wild-type, MEFs argues that Stk11 plays an important regulatory role in limiting ciliary disassembly and that chemicals targeting HDAC6 may be useful in restoring some aspects of Stk11-induced pathology (Fig. 6G).

Our study suggests that sequestration of Dvl away from Wnt receptors represents an important checkpoint in Wnt pathway responses and that this checkpoint may be lost in Stk11-associated tumors. About two-thirds of cervical carcinomas exhibit increased abundance of Dvl protein (41), suggesting that increased Dvl activity may be a common defect in this cancer type. Given the role of Dvl in mediating a diverse array of Wnt-dependent responses, our findings reveal a mechanistic basis underlying deviant Wnt-dependent transcriptional response and possibly other Wnt-associated cellular derangements in cancerous cells lacking Stk11 (42). Thus, inhibitors of Wnt production, such as the Porcn inhibitors, may be useful in some Stk11-associated cancers, whereas inhibitors of canonical Wnt responses, such as those that induce Axin stability, may be additionally relevant in a subset of such cancers (Fig. 6G).

Given the tremendous resources devoted to achieving chemical control of the Hh and Wnt pathways for therapeutic goals, our screening strategy potentially broadens the number of diseases that may be managed with modulators of these pathways. We focused here on the role of Hh and Wnt signaling in Stk11-associated tumors; however, further studies are required to understand the nature of other disease-pathway relationships established in our screen. Our identification of chemical means to counter some of the effects resulting from loss of a multitasking gene product, such as Stk11, suggests that screening additional signal transduction pathways with this approach would further facilitate the deconstruction and, ultimately, management of complex diseases.

MATERIALS AND METHODS

Reagents

3T3-ShhFL cells used in the primary screen were generated by the stable transfection of NIH 3T3 cells expressing Shh protein (provided by P. A. Beachy) with a Hh-responsive reporter [8x-Gli-BS-Luc (43)], and a *Renilla* luciferase (RL) reporter, pRL-SV40 (Promega). ShhLightII cells (12), HeLa cells, NIH 3T3 cells, and DLD-1 cells were purchased from the American Type Culture Collection. Wild-type MEFs and *STK11*$^{-/-}$ MEFs were provided by N. Bardeesy, *IFT88*$^{-/-}$ MEFs by A. Liu, and *PRKAR1A*$^{-/-}$ MEFs by L. Kirschner. HBEC cells were provided by J. Shay. Lung cancer cell lines H1819, H460, A549, and H23 were provided by J. Minna. Endo and SiHa cells were provided by D. Castrillon.

The human STK11 (NM_000455) expression construct was purchased from Origene. KD STK11 (STK11 K78M) was engineered with polymerase chain reaction (PCR)–based cloning and mutagenesis strategies. The STF reporter plasmid was provided by R. T. Moon. The pRK5-ShhN and Wnt3A plasmids were provided by P. A. Beachy. Axin1-GFP and Dvl2-GFP plasmids were provided by M. Bienz.

SAG was purchased from Alexis Biochemicals, D4476 from Tocris, and Sant1 from Sigma. IWP and IWR compounds targeting the Wnt pathway components Porcupine and Tankyrase, respectively, were synthesized de novo as previously described (29). The HDAC inhibitor SAHAwas provided by C. Chen. Tubacin (a specific HDAC6 inhibitor) and

MS-275 (HDAC1-3 inhibitor) were provided by R. Mazitschek and S. Schreiber. 5-(Tetradecyloxy)-2-furoic acid (TOFA) was purchased from Cayman Chemicals.

The antibody that recognizes Gli3 was obtained from Genentech (6F5), B. Wang, or R&D Systems. The antibody against Prkar1a was purchased from BD Biosciences. The antibody that recognizes Smo was provided by J. Kim and P. A. Beachy. Antibodies against acetylated tubulin, □catenin, and □actin were purchased from Sigma. Antibodies against Stk11, Dvl2, Axin1, Axin2, p-ERK, p-LRP6, LRP6, Dvl3, and □-tubulin were purchased from Cell Signaling Technologies. Antibodies against Dvl1 and Tnks 1/2 were purchased from Santa Cruz Biotechnology. The antibody that recognizes GFP was purchased from MBL.

Nonsilencing siRNAs (AllStars Negative Control siRNA) were purchased from Qiagen. Sequences of siRNAs used in secondary tests are in table S5.

Screening

Mouse genome-wide siRNA libraries, produced by Dharmacon and Qiagen, were screened by transfecting siRNA pools targeting a single gene into 3T3-ShhFL cells in 96-well format with the X-tremeGENE transfection reagent (Roche), according to the manufacturer's protocol. The final siRNA concentration was 57 nM. Twenty-four hours after transfection, cells were placed under low-serum conditions (0.5% calf serum). Seventy-two hours after transfection, firefly luciferase (FL) and RL activities were assessed with the Dual-Luciferase kit (Promega). To account for edge effects and variation across plates, we normalized luciferase measurements to the average luciferase value for each well position across all plates and to the average luciferase measurement of each plate. Samples for which the triplicate data were inconsistent (SD >0.1) were removed from consideration. *z* scores were calculated by determining the number of SDs that the luciferase measurements for each siRNA pool fell away from the mean values for all the siRNA pools in each primary screen. siRNA pools that affected the RL control reporter ($|z| > 2.5$) were removed from consideration. siRNA pools for which FL $z \leq -2.0$ (97.73% confidence) were further evaluated by secondary screens.

The exogenous Shh secondary screen was performed essentially as above by the transfection of ShhLightII cells with siRNAs and, 24 hours later, the addition of ShhN-conditioned media, collected from human embryonic kidney (HEK) 293–ShhN cells. Average FL measurements ≤75% of FL for nonsilencing siRNA controls and SD <0.15 were considered for further testing. The Wnt counterscreen was performed by transfection of NIH 3T3 cells with the STF reporter, the RL reporter, the Wnt3A plasmid, and siRNAs using the Effectene transfection reagent (Qiagen), according to the manufacturer's protocol. Final siRNA concentration was 25 nM. The low-throughput counterscreen (cross-library test) was performed by hand in 96-well format with only the center wells of the plate. The RNAi specificity test was performed in the same manner as the exogenous Shh secondary test with individual siRNAs (table S5).

RT-PCR and qPCR

Reverse transcription PCR (RT-PCR) analysis was performed as previously described (19). Primer design for RT-PCR was as follows: GapDH forward (F), ATCCTGCACCACCAACT; GapDH reverse (R), TGCCTGCTTCA-CCACCTT; Ptch1 F, ACTGTCCAGCTACCCCAATG; and Ptch1 R, CAT-CATGCCAAAGAGCTCAA. Quantitative PCR (qPCR) analysis primers were as follows: GapDH F, ACATCGCTCAGACACCATG; GapDH R, TGTAGTTGAGGTCAATGAAGGG; Gli3 F, GGGATTCCGACAGTT-CTGAACC; Gli3 R, CTGGGGAGGTCTTCATCAGGC; Ptch F,

CGTCAGAAGATAGGAGAAGAGGC; and Ptch R, GTAGCACAAA-TGTTCCAACTTCC.

Analysis of GliR formation and degradation

Gli3R formation was inhibited by addition of either Shh-conditioned medium or SAG (0.2 μM) for 24 hours. Conditioned medium or SAG was then removed and replaced with a medium containing Smo antagonist (SANT, 2.5 μM) to inhibit Shh pathway response and to allow reinitiation of Gli3R formation. Cellular lysate was then collected at indicated time points. To examine the rate of Gli3R turnover, we treated cells with MG132 to inhibit proteasome-dependent Gli processing. Cellular lysate was then collected at various time points. Samples were analyzed by Western blot, and Gli3R protein was quantified with ImageJ or Gene Tools software.

Zebrafish experiments

Wild-type zebrafish embryos were injected with 3 pmol of MO targeting STK11 (sequence: GAGATCCGCGCCCACGCTCATCTTT) or standard control (Gene Tools) at the one- to two-cell stage. Whole-mount in situ hybridization was performed at 24 hours after fertilization with digoxigenin-labeled antisense RNA probes generated against *Eng1A* (BC080209; base pairs 3 to 1433), *Axin2* (BC045281; base pairs 341 to 1144), or *MyoD* (NM_131262; base pairs 316 to 927).

Transmission electron microscopy

Cells were fixed in 2.5% glutaraldehyde in 0.1 M sodium cacodylate buffer, postfixed in buffered 1% osmium tetroxide, en bloc–stained in 2% uranyl acetate, dehydrated with a graded series of ethanol, and embedded in EMbed-812 resin. Thin sections were cut on a Leica Ultracut UCT ultramicrotome and then stained with 2% uranyl acetate and lead citrate. Images were acquired on an FEI Tecnai G2 Spirit electron microscope equipped with a LaB6 source and operating at 120 kV.

RNAi and overexpression studies in cultured cells

For studies involving transfection of siRNAs, DharmaFECT 3 (Dharmacon), Effectene (Qiagen), or X-tremeGENE (Roche) reagent was used per the manufacturer's protocol. For studies involving transfection of complementary DNAs (cDNAs), FuGENE HD (Roche) or Effectene (Qiagen) was used according to the manufacturer's instructions.

Western blot analysis and immunofluorescence

Cell lysates for Western blot analysis were generated with either phosphate-buffered saline (PBS)/1% NP-40 or RIPA (radioimmunoprecipitation assay) buffer (for detection of Gli proteins). Western blot results were quantified with ImageJ or Gene Tools software. For imaging of cilia, cells were plated at high density and low serum on polylysinecoated coverslips (BD Biosciences). In experiments with SAHA or IWP, cells were treated for 24 hours. For Smo localization experiments, cells were treated with ShhN-conditioned media for 4 hours before fixation. Cells were fixed in either 4% formaldehyde or ice-cold methanol and incubated with antibody against acetylated tubulin and then secondary antibodies (mouse fluorescein isothiocyanate–conjugated or Alexa Fluor 488–conjugated antibodies) diluted in PBS, 0.2% Triton X-100, and 5% goat serum. Cilia were imaged and measurements were taken with Adobe Photoshop.

Cancer cell growth studies

Cancer cell growth studies were performed as previously described (29). Briefly, cells were seeded at clonal density (1500 cells in 24-well format) and cellular adenosine 5 triphosphate (ATP) levels were measured 6 days later with CellTiter-Glo reagent (Promega).

Supplementary Material

Refer to Web version on PubMed Central for supplementary material.

Acknowledgments

We thank N. Bardeesy, J. Kim, P. Beachy, A. Liu, L. Kirschner, D. Castrillon, R. Mazitschek, S. Schreiber, J. Shay, J. Minna, C. Chen, and S. Scales for reagents. We also thank B. Perkins, C. Gilpin, K. Luby-Phelps, T. Carroll, L. Huang, and U. Eskiocak for technical assistance. We thank J. K. Chen and colleagues for useful discussions. Finally, we thank members of the Lum lab and W. Snell for critical reading of this manuscript.

Funding: This work was supported by the NIH (1R01GM076398), the American Cancer Society (RSG GMC-07-062-01), the Welch Foundation (I-1665), and an endowment from Virginia Murchinson Linthicum to L.L.

REFERENCES AND NOTES

1. Jiang J, Hui CC. Hedgehog signaling in development and cancer. Dev Cell. 2008; 15:801–812. [PubMed: 19081070]
2. MacDonald BT, Tamai K, He X. Wnt/ catenin signaling: Components, mechanisms, and diseases. Dev Cell. 2009; 17:9–26. [PubMed: 19619488]
3. Barker N, Clevers H. Mining the Wnt pathway for cancer therapeutics. Nat Rev Drug Discov. 2006; 5:997–1014. [PubMed: 17139285]
4. Rubin LL, de Sauvage FJ. Targeting the Hedgehog pathway in cancer. Nat Rev Drug Discov. 2006; 5:1026–1033. [PubMed: 17139287]
5. Jacob L, Lum L. Deconstructing the Hedgehog pathway in development and disease. Science. 2007; 318:66–68. [PubMed: 17916724]
6. Moon RT. Wnt/ catenin pathway. Sci STKE. 2005; 2005:cm1. [PubMed: 15713948]
7. Goetz SC, Anderson KV. The primary cilium: A signalling centre during vertebrate development. Nat Rev Genet. 2010; 11:331–344. [PubMed: 20395968]
8. Haycraft CJ, Banizs B, Aydin-Son Y, Zhang Q, Michaud EJ, Yoder BK. Gli2 and Gli3 localize to cilia and require the intraflagellar transport protein Polaris for processing and function. PLoS Genet. 2005; 1:e53. [PubMed: 16254602]
9. Liu A, Wang B, Niswander LA. Mouse intraflagellar transport proteins regulate both the activator and repressor functions of Gli transcription factors. Development. 2005; 132:3103–3111. [PubMed: 15930098]
10. May SR, Ashique AM, Karlen M, Wang B, Shen Y, Zarbalis K, Reiter J, Ericson J, Peterson AS. Loss of the retrograde motor for IFT disrupts localization of Smo to cilia and prevents the expression of both activator and repressor functions of Gli. Dev Biol. 2005; 287:378–389. [PubMed: 16229832]
11. Sharma N, Berbari NF, Yoder BK. Ciliary dysfunction in developmental abnormalities and diseases. Curr Top Dev Biol. 2008; 85:371–427. [PubMed: 19147012]
12. Taipale J, Chen JK, Cooper MK, Wang B, Mann RK, Milenkovic L, Scott MP, Beachy PA. Effects of oncogenic mutations in Smoothened and Patched can be reversed by cyclopamine. Nature. 2000; 406:1005–1009. [PubMed: 10984056]
13. Tang W, Dodge M, Gundapaneni D, Michnoff C, Roth M, Lum L. A genome-wide RNAi screen for Wnt/ catenin pathway components identifies unexpected roles for TCF transcription factors in cancer. Proc Natl Acad Sci USA. 2008; 105:9697–9702. [PubMed: 18621708]
14. Evangelista M, Lim TY, Lee J, Parker L, Ashique A, Peterson AS, Ye W, Davis DP, de Sauvage FJ. Kinome siRNA screen identifies regulators of ciliogenesis and Hedgehog signal transduction. Sci Signal. 2008; 1:ra7. [PubMed: 18827223]

15. Lum L, Yao S, Mozer B, Rovescalli A, Von Kessler D, Nirenberg M, Beachy PA. Identification of Hedgehog pathway components by RNAi in *Drosophila* cultured cells. Science. 2003; 299:2039–2045. [PubMed: 12663920]

16. Krock BL, Perkins BD. The intraflagellar transport protein IFT57 is required for cilia maintenance and regulates IFT-particle–kinesin-II dissociation in vertebrate photoreceptors. J Cell Sci. 2008; 121:1907–1915. [PubMed: 18492793]

17. Maw MA, Kennedy B, Knight A, Bridges R, Roth KE, Mani EJ, Mukkadan JK, Nancarrow D, Crabb JW, Denton MJ. Mutation of the gene encoding cellular retinaldehyde-binding protein in autosomal recessive retinitis pigmentosa. Nat Genet. 1997; 17:198–200. [PubMed: 9326942]

18. Hezel AF, Bardeesy N. LKB1; linking cell structure and tumor suppression. Oncogene. 2008; 27:6908–6919. [PubMed: 19029933]

19. Wang B, Fallon JF, Beachy PA. Hedgehog-regulated processing of Gli3 produces an anterior/posterior repressor gradient in the developing vertebrate limb. Cell. 2000; 100:423–434. [PubMed: 10693759]

20. Bardeesy N, Sinha M, Hezel AF, Signoretti S, Hathaway NA, Sharpless NE, Loda M, Carrasco DR, DePinho RA. Loss of the Lkb1 tumour suppressor provokes intestinal polyposis but resistance to transformation. Nature. 2002; 419:162–167. [PubMed: 12226664]

21. Pugacheva EN, Jablonski SA, Hartman TR, Henske EP, Golemis EA. HEF1-dependent Aurora A activation induces disassembly of the primary cilium. Cell. 2007; 129:1351–1363. [PubMed: 17604723]

22. Carey N, La Thangue NB. Histone deacetylase inhibitors: Gathering pace. Curr Opin Pharmacol. 2006; 6:369–375. [PubMed: 16781195]

23. Humke EW, Dorn KV, Milenkovic L, Scott MP, Rohatgi R. The output of Hedgehog signaling is controlled by the dynamic association between Suppressor of Fused and the Gli proteins. Genes Dev. 2010; 24:670–682. [PubMed: 20360384]

24. Kim J, Kato M, Beachy PA. Gli2 trafficking links Hedgehog-dependent activation of Smoothened in the primary cilium to transcriptional activation in the nucleus. Proc Natl Acad Sci USA. 2009; 106:21666–21671. [PubMed: 19996169]

25. Wen X, Lai CK, Evangelista M, Hongo JA, de Sauvage FJ, Scales SJ. Kinetics of hedgehog-dependent full-length Gli3 accumulation in primary cilia and subsequent degradation. Mol Cell Biol. 2010; 30:1910–1922. [PubMed: 20154143]

26. Corbit KC, Aanstad P, Singla V, Norman AR, Stainier DY, Reiter JF. Vertebrate Smoothened functions at the primary cilium. Nature. 2005; 437:1018–1021. [PubMed: 16136078]

27. Rohatgi R, Milenkovic L, Scott MP. Patched1 regulates Hedgehog signaling at the primary cilium. Science. 2007; 317:372–376. [PubMed: 17641202]

28. Bryja V, Schulte G, Rawal N, Grahn A, Arenas E. Wnt-5a induces Dishevelled phosphorylation and dopaminergic differentiation via a CK1-dependent mechanism. J Cell Sci. 2007; 120:586–595. [PubMed: 17244647]

29. Chen B, Dodge ME, Tang W, Lu J, Ma Z, Fan CW, Wei S, Hao W, Kilgore J, Williams NS, Roth MG, Amatruda JF, Chen C, Lum L. Small molecule–mediated disruption of Wnt-dependent signaling in tissue regeneration and cancer. Nat Chem Biol. 2009; 5:100–107. [PubMed: 19125156]

30. Gao C, Chen YG. Dishevelled: The hub of Wnt signaling. Cell Signal. 2010; 22:717–727. [PubMed: 20006983]

31. Schwarz-Romond T, Metcalfe C, Bienz M. Dynamic recruitment of axin by Dishevelled protein assemblies. J Cell Sci. 2007; 120:2402–2412. [PubMed: 17606995]

32. Marlow F, Gonzalez EM, Yin C, Rojo C, Solnica-Krezel L. No tail co-operates with non-canonical Wnt signaling to regulate posterior body morphogenesis in zebrafish. Development. 2004; 131:203–216. [PubMed: 14660439]

33. Wolff C, Roy S, Ingham PW. Multiple muscle cell identities induced by distinct levels and timing of hedgehog activity in the zebrafish embryo. Curr Biol. 2003; 13:1169–1181. [PubMed: 12867027]

34. Sanchez-Cespedes M, Parrella P, Esteller M, Nomoto S, Trink B, Engles JM, Westra WH, Herman JG, Sidransky D. Inactivation of LKB1/STK11 is a common event in adenocarcinomas of the lung. Cancer Res. 2002; 62:3659–3662. [PubMed: 12097271]

35. Wingo SN, Gallardo TD, Akbay EA, Liang MC, Contreras CM, Boren T, Shimamura T, Miller DS, Sharpless NE, Bardeesy N, Kwiatkowski DJ, Schorge JO, Wong KK, Castrillon DH. Somatic LKB1 mutations promote cervical cancer progression. PLoS One. 2009; 4:e5137. [PubMed: 19340305]

36. Alieva IB, Gorgidze LA, Komarova YA, Chernobelskaya OA, Vorobjev IA. Experimental model for studying the primary cilia in tissue culture cells. Membr Cell Biol. 1999; 12:895–905. [PubMed: 10512057]

37. van Amerongen R, Nusse R. Towards an integrated view of Wnt signaling in development. Development. 2009; 136:3205–3214. [PubMed: 19736321]

38. Caspary T, Larkins CE, Anderson KV. The graded response to Sonic Hedgehog depends on cilia architecture. Dev Cell. 2007; 12:767–778. [PubMed: 17488627]

39. Ko HW, Norman RX, Tran J, Fuller KP, Fukuda M, Eggenschwiler JT. Broad-minded links cell cycle-related kinase to cilia assembly and Hedgehog signal transduction. Dev Cell. 2010; 18:237–247. [PubMed: 20159594]

40. Tran PV, Haycraft CJ, Besschetnova TY, Turbe-Doan A, Stottmann RW, Herron BJ, Chesebro AL, Qiu H, Scherz PJ, Shah JV, Yoder BK, Beier DR. THM1 negatively modulates mouse sonic hedgehog signal transduction and affects retrograde intraflagellar transport in cilia. Nat Genet. 2008; 40:403–410. [PubMed: 18327258]

41. Okino K, Nagai H, Hatta M, Nagahata T, Yoneyama K, Ohta Y, Jin E, Kawanami O, Araki T, Emi M. Up-regulation and overproduction of DVL-1, the human counterpart of the *Drosophila* dishevelled gene, in cervical squamous cell carcinoma. Oncol Rep. 2003; 10:1219–1223. [PubMed: 12883684]

42. Lai SL, Chien AJ, Moon RT. Wnt/Fz signaling and the cytoskeleton: Potential roles in tumorigenesis. Cell Res. 2009; 19:532–545. [PubMed: 19365405]

43. Sasaki H, Hui C, Nakafuku M, Kondoh H. A binding site for Gli proteins is essential for *HNF-3b* floor plate enhancer activity in transgenics and can respond to Shh in vitro. Development. 1997; 124:1313–1322. [PubMed: 9118802]

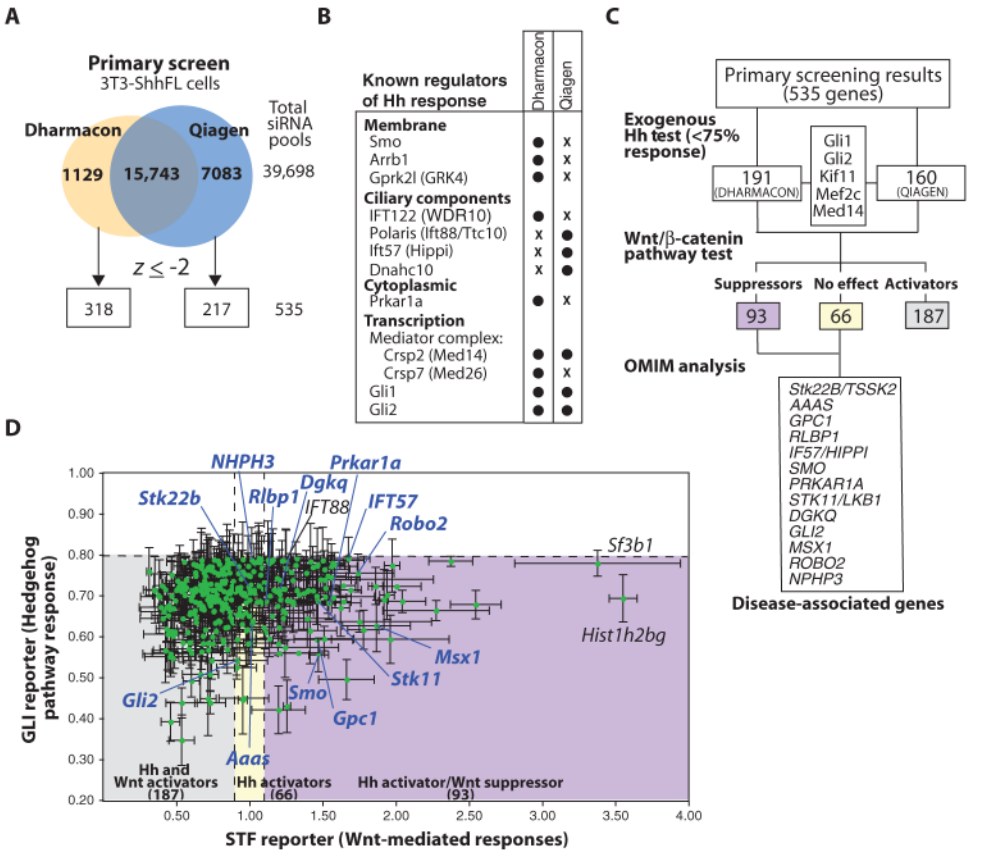

Fig. 1.

A genome-scale screen to identify Hh signal transducing genes. (**A**) siRNA libraries designed by Dharmacon or Qiagen were screened in triplicate using the 3T3-ShhFL cells. (**B**) Many known Hh pathway components were identified with siRNAs from a single library. (**C**) Genes identified from the primary screen were retested using NIH 3T3 cells stably harboring the GliBS reporter (ShhLightII cells) in the presence of culture medium containing ShhN (“Exogenous Hh test”). siRNAs that retained their activity in this assay were tested with the STF reporter in NIH 3T3 cells transfected with Wnt3A cDNA to assign function in the Wnt/ □catenin pathway. Genes with no activity or suppressor function in this pathway were cross-referenced with the OMIM database to identify disease-associated genes (Table 1). Multiple names for a single gene are separated by a slash. (**D**) Graphical summary of gene function in the Hh (*y* axis) and Wnt/ □catenin (*x* axis) pathways. Disease-associated genes (blue) are noted along with other genes of interest (black).

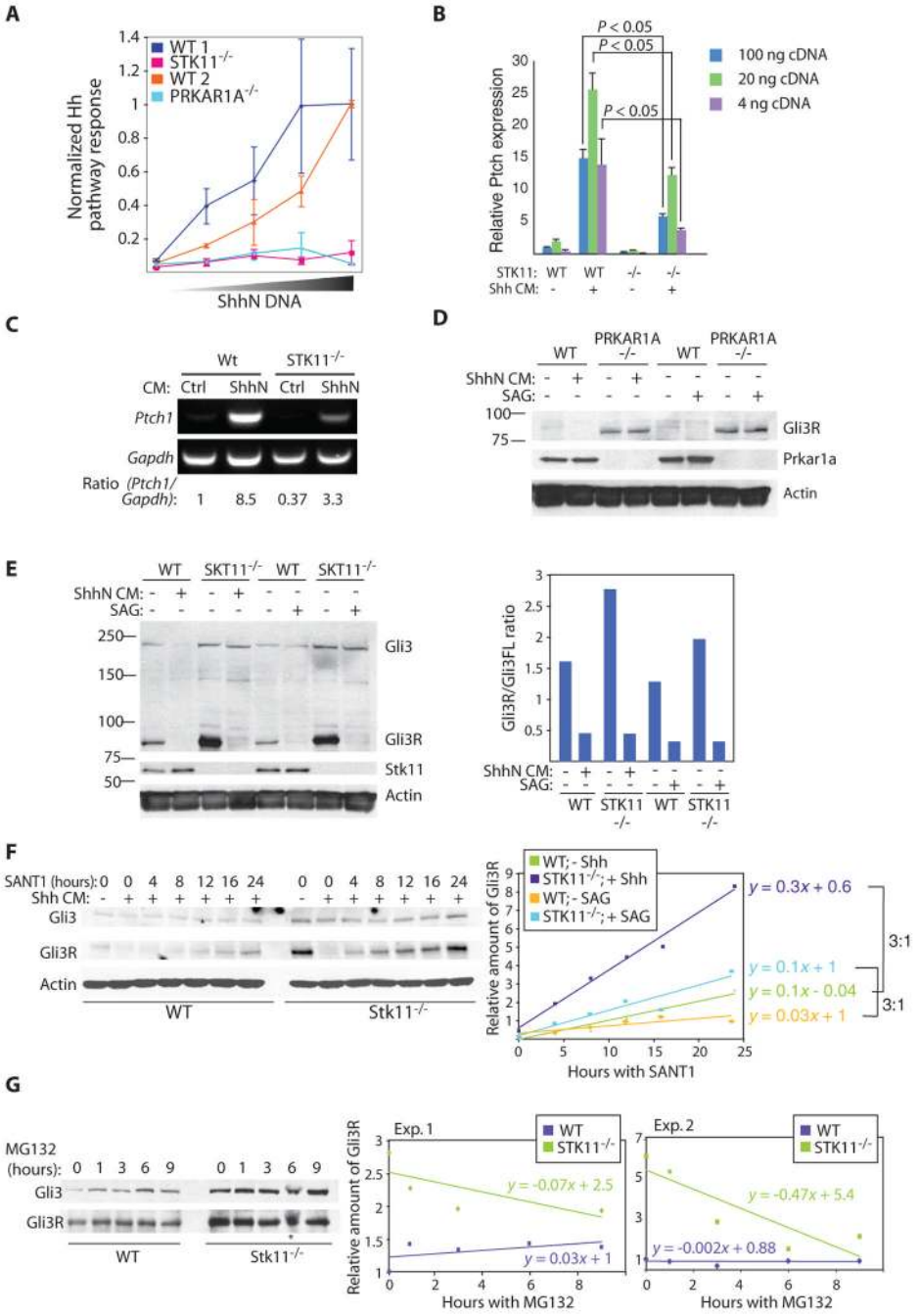

Fig. 2.

Loss of Hh pathway response induced by compromised Stk11 or Prkar1a function is associated with increased abundance of GliR. (**A**) MEFs null for either *STK11* or *PRKAR1A* fail to achieve normal levels of Hh pathway response. MEFs were transfected with the GliBS and control reporters and increasing amounts of ShhN cDNA. Mean and SD are shown. The experiment was performed in triplicate. (**B**) *STK11*$^{-/-}$ MEFs have dampened transcriptional response to exogenous ShhN. qPCR analysis of *Ptch1* expression in wild-type (WT) and *STK11*$^{-/-}$ MEFs in the presence or absence of Shh stimulation. PCR was performed from different concentrations of total cDNA generated from RNA samples,

analyzed, and compared to test reproducibility. *Ptch1* transcript abundance was normalized to *Gapdh* (glyceraldehyde-3-phosphate dehydrogenase). Graph shows mean and SD from three samples. (**C**) RT-PCR–based confirmation of qPCR results. *Ptch1* RT-PCR results from WT and $STK11^{-/-}$ cells in the presence and absence of Shh-conditioned medium (CM) also show reduced responsiveness of $STK11^{-/-}$ cells to Shh. (**D**) MEFs deficient in Prkar1a exhibit increased formation of Gli3R, even in the presence of Hh signaling mediated by addition of ShhN CM or SAG, as measured with Western blot analysis. Data shown are representative of two experiments. (**E**) Stk11 regulates Gli3R abundance. $STK11^{-/-}$ MEFs exhibit increased abundance of Gli3R that is inhibited by Hh pathway activation. Graph shows quantification of results by densitometry. A representative of three independent experiments is shown. (**F**) $STK11^{-/-}$MEFs exhibit an accelerated rate of Gli3R accumulation. WT or $STK11^{-/-}$ MEFs were treated with Shh CM overnight to inhibit Gli3 processing. Shh CM was then removed and replaced with the Smo inhibitor SANT1 to allow processing to proceed. Cells were lysed at indicated time points. Quantification (right) indicates that the rate of Gli3R accumulation is three times faster in the absence of Stk11 as calculated from two independent experiments (one with Shh CM and another with SAG to inhibit Gli3R formation; see fig. S3B). Rate of Gli3R formation was calculated from the slope of each line. Gli3R abundance is calculated relative to abundance of Gli3R in WT cells at 0 hours of SANT1 treatment in the absence of Shh CM or SAG. (**G**) Gli3R destruction is accelerated rather than slowed in $STK11^{-/-}$ MEFs. WT or $STK11^{-/-}$ MEFs were treated with the proteasome inhibitor MG132 for various time periods to restrict new formation of Gli3R by proteasome-dependent proteolytic processing. Gli3R abundance was determined by Western blot analysis and quantified by normalizing to Gli3R in WT cells in the absence of MG132. The asterisk indicates result not used for quantification. Data shown are representative of two experiments.

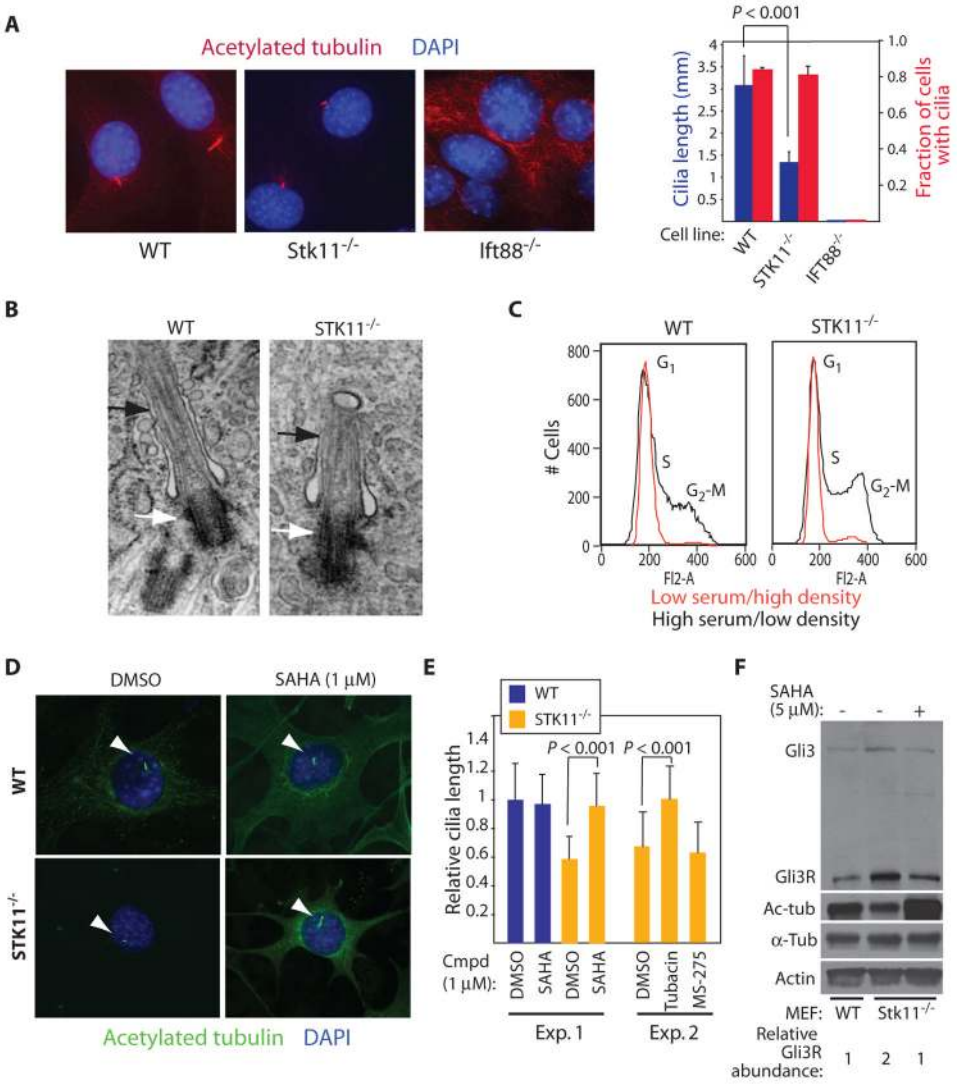

Fig. 3.

Stk11 is required for primary cilia maintenance in embryonic fibroblasts. (**A**) MEFs were immunostained for acetylated tubulin to detect the primary cilium. Unlike cells lacking the ciliary component IFT88, a rudimentary primary cilium is observed in *STK11*$^{-/-}$ cells. Cells lacking Stk11 do not have a defect in establishing cilia. MEFs of the indicated genotype were scored for the presence of cilia and cilia length by immunofluorescence. Data show the mean and SD of >35 cells per condition. (**B**) Ultrastructural analysis of the primary cilium in *STK11*$^{-/-}$ cells by transmission electron microscopy. No gross defects in the basal body (white arrows) and axoneme (black arrows) are observed in *STK11*$^{-/-}$cells. Image of *STK11*$^{-/-}$ cilia is representative of four samples. (**C**) WT and *STK11*$^{-/-}$ MEFs show comparable cell cycle response to serum and cell density. Cells were grown in either high-serum/low-density conditions or low-serum/high-density conditions for 24 hours, stained with propidium iodide, and subjected to FACS (fluorescence-activated cell sorting) analysis. (**D**) HDAC inhibition restores primary cilium length in *STK11*$^{-/-}$ cells. MEFs treated with the nonselective HDAC inhibitor SAHA were stained for acetylated tubulin. DMSO, dimethyl sulfoxide. (**E**) HDAC6 inhibition restores primary cilium of *STK11*$^{-/-}$ cells to normal length. Quantification of results in (D) (Exp. 1) and analysis of the specific HDAC6

inhibitor tubacin and the HDAC1 inhibitor MS-275 on cilia length in *STK11*$^{-/-}$ cells (Exp. 2). Fifty cells were counted in each experiment. (**F**) SAHA treatment of *STK11*$^{-/-}$ MEFs reduces the abundance of Gli3R. Abundance of Gli3R relative to actin was quantified by Western blot analysis and normalized to WT sample. Acetylated tubulin abundance serves as a positive control for SAHA activity. Data are representative of three experiments.

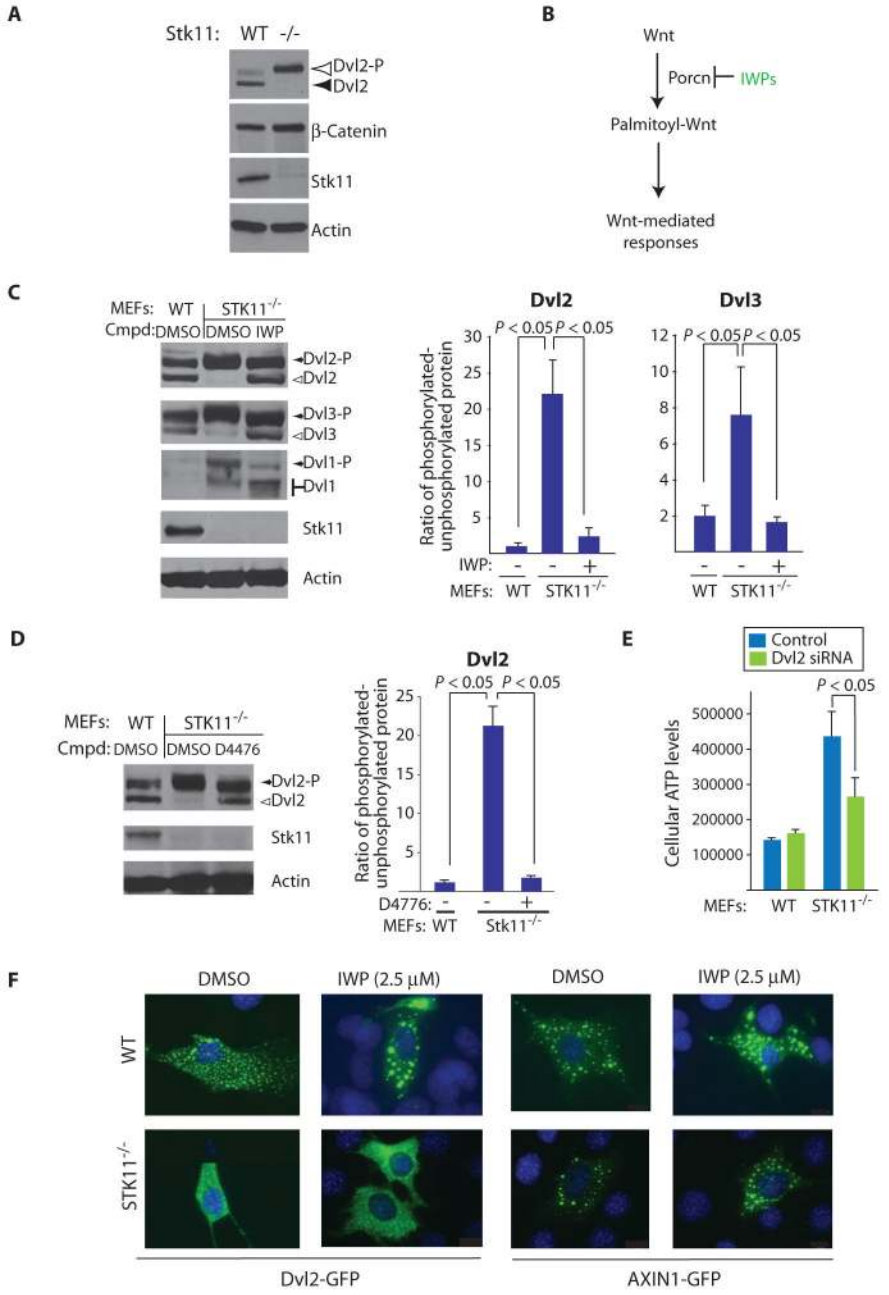

Fig. 4.

Loss of Stk11 engages aberrant Wnt-dependent cellular responses. (**A**) Phosphorylated Dvl2 is abundant in MEFs lacking Stk11. Data are representative of three experiments. (**B**) The IWP compound inhibits Porcupine (Porcn), an acyltransferase essential for Wnt protein production. (**C**) Increased Dvl2 and Dvl3 phosphorylation in *STK11*$^{-/-}$ cells is inhibited by IWP (2.5 □M), indicating that Dvl phosphorylation is dependent on production of Wnt. Results performed from three independent experiments are quantified. The abundance of Dvl1 is increased in *STK11*$^{-/-}$ cells compared to WT cells, and the relative abundance of phosphorylated/unphosphorylated proteins was not quantified. (**D**) Application of the CK1 inhibitor D4476 (0.2 mM) to *STK11*$^{-/-}$ cells inhibits Dvl2 phosphorylation. Data are representative of three experiments. (**E**) Loss of Dvl2 inhibits growth of *STK11*$^{-/-}$ cells.

MEFs transfected with Dvl2 siRNAs were plated at clonal density, and CellTiter-Glo assay was performed after 6 days. Data show the mean and SD of three samples. (**F**) Loss of Stk11 is associated with mislocalization of Dvl2. MEFs, transfected with either Dvl2-GFP or Axin1-GFP DNA, were treated with DMSO or IWP. Green, GFP; blue, DAPI (4′,6-diamidino-2-phenylindole). Images were taken at 40× magnification.

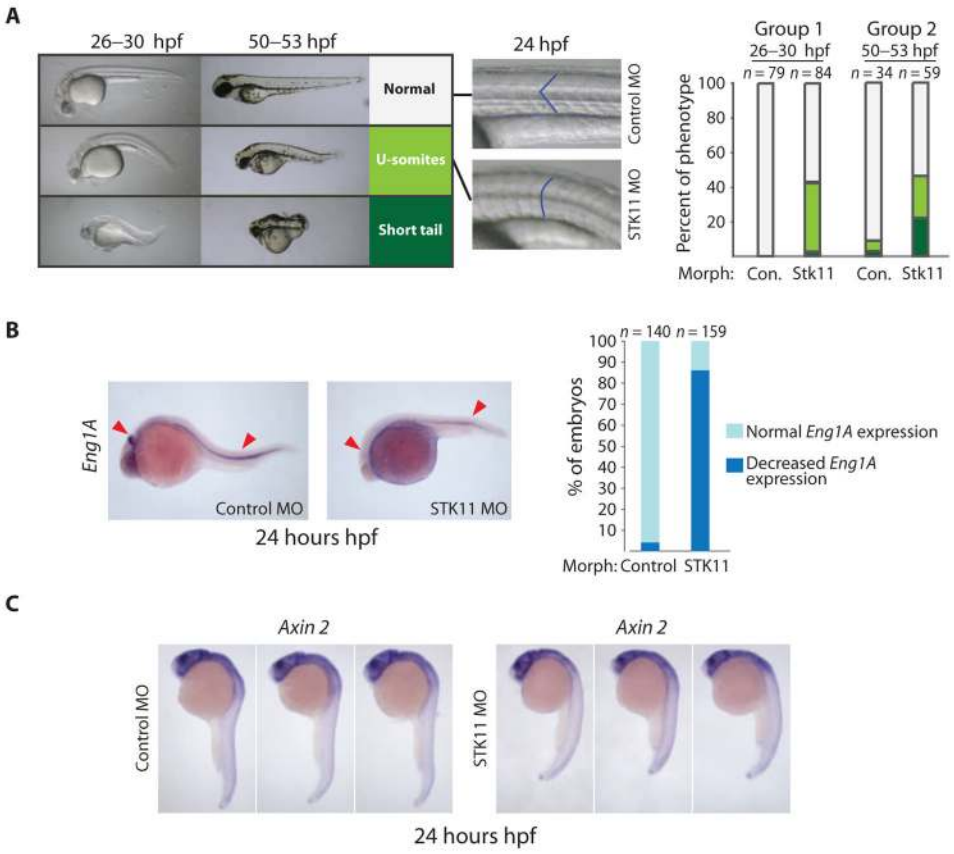

Fig. 5.

Zebrafish embryos in which Stk11 is reduced exhibit phenotypes consistent with Hh and Wnt signaling defects. (**A**) Zebrafish injected with MO against STK11 show U-shaped somites, shortened tails, or no detectable change in body patterning. Phenotypic analysis was performed at two different developmental stages (groups 1 and 2) in separate experiments. The left side shows representative embryos of each phenotype and the right side shows quantification. hpf, hours postfertilization. (**B**) Loss of Stk11 reduces expression of *Engrailed 1A* (*Eng1A*), a target gene induced by Hh signaling. Quantification of embryos with decreased *Eng1A* expression at the midbrain-hindbrain boundary and muscle pioneers. In situ hybridization with digoxigenin-labeled antisense probes against *Eng1a* mRNA was performed at 24 hpf embryos. More than 100 animals were scored in each condition. (**C**) STK11 morphants exhibit little change in *Axin2* expression when compared to control animals. In situ hybridization with digoxigenin-labeled antisense probes against *Axin2* mRNA was performed at 24 hpf embryos that had been injected with control MO or STK11 MO. Representative embryos from 30 animals analyzed in each group are shown.

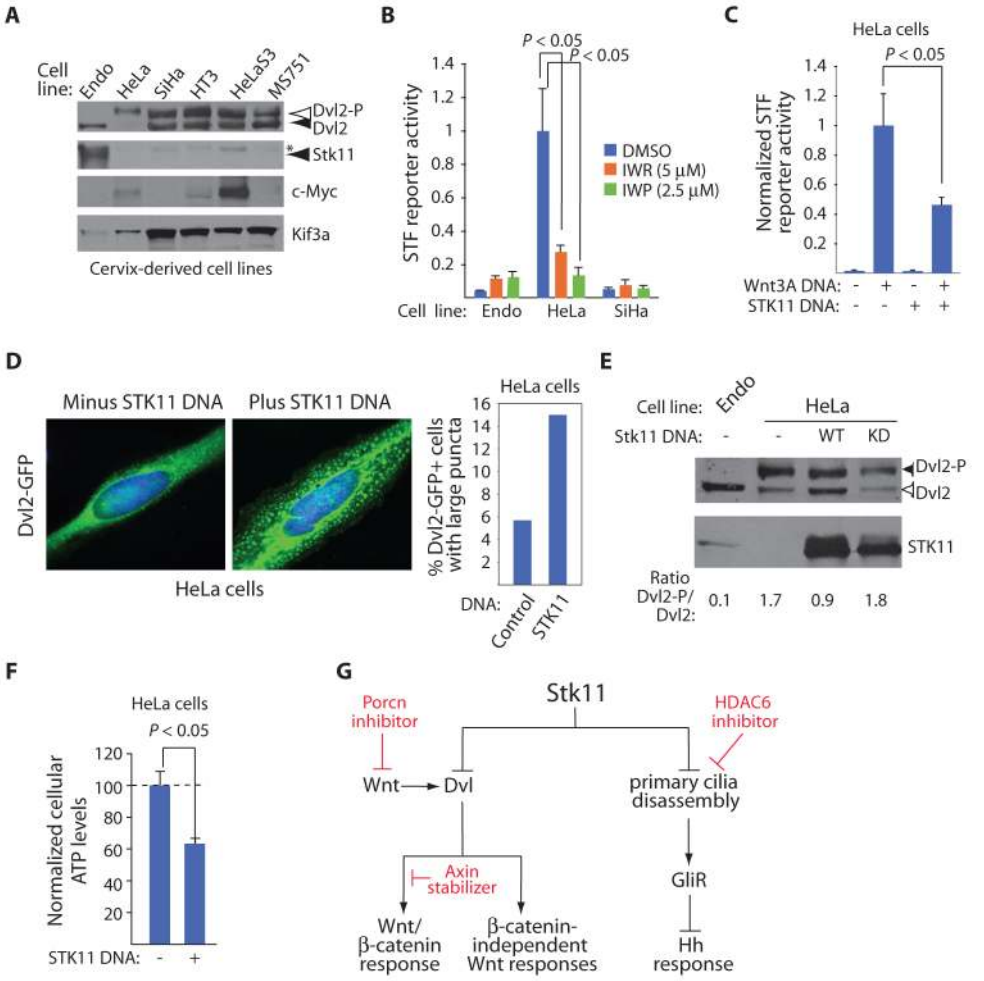

Fig. 6.

Loss of Stk11 results in deviant Wnt-mediated responses in cancer cell lines. (**A**) Cervical carcinoma cells lacking Stk11 exhibit increased abundance of phosphorylated Dvl2 but not necessarily activation of the canonical Wnt/ β-catenin pathway. Lysates from cervical carcinoma cell lines or normal endometrial cells (Endo cells) were Western-blotted for Dvl2, Stk11, or c-Myc, the product of a Wnt/ β-catenin target gene. Kif3a is a loading control. The asterisk indicates background band. (**B**) Wnt/ β-catenin pathway activity in HeLa cells is sensitive to disruption of Wnt production or inhibition of the canonical Wnt pathway. Endo, HeLa, or SiHA cells transfected with the STF reporter were treated with either IWP or IWR compounds. Data show the mean and SD of three samples. (**C**) Stk11 disrupts Wnt/ β-catenin response in HeLa cells. STF reporter was transfected with or without Wnt3A and Stk11 DNA into HeLa cells. Data show the mean and SD of three samples. (**D**) Introduction of Stk11 increases the number of HeLa cells with punctate Dvl2 localization. Dvl2-GFP protein in HeLa cells shows a diffuse localization pattern, similar to that observed in *STK11*$^{-/-}$ MEFs. By contrast, the Dvl binding partner Axin1 exhibits a punctate expression pattern (fig. S10). Cells were transfected with Dvl2-GFP DNA with or without Stk11 DNA. $n = 50$ for each condition. (**E**) Kinase activity of Stk11 is required for suppression of Dvl2 activity. Expression constructs encoding wild-type or a K78M mutant (kinase-dead, KD) form of Stk11 were transfected into HeLa cells, and effects on Dvl2 phosphorylation were analyzed by Western blotting. Data are representative of three independent experiments. (**F**) Introduction of Stk11 in HeLa cells inhibits cell growth. Transfected cells were seeded at

clonal density. The amount of cellular ATP was determined as a measure of cell number after 5 days. Data show the mean and SD of three samples. (**G**) Chemically tractable mechanisms underlying aberrant Hh and Wnt pathway responses in *STK11*-null cells. HDAC6 inhibitors, such as SAHA or tubacin, could restore normal cilia length and the abundance of GliR molecules. Porcn and Axin stabilizers that respectively inhibit Wnt protein production and induce □catenin destruction could be used to counter the effects of excess Dvl activation.

Table 1

Disease-associated genes with potential roles in Hh and Wnt signaling. Disease-associated genes that were confirmed by siRNA retesting (either by two nonredundant siRNA pools or by three or more individual siRNAs; see fig. S2) were grouped on the basis of disease type. NC, no change; +, gain in response (normalized response >1.2; see table S4). Multiple names for a single gene are separated by a slash.

Pathological condition	Gene	Function	Associated disease	RNAi specificity test	Wnt pathway response
Malformation	*G1i2*	Transcription	Holoprosencephaly	2x pools	NC
	Stk22B/Tssk2	Kinase	DiGeorge syndrome candidate gene (velocardiofacial syndrome)	2x pools	NC
	Dgkq	Kinase	Wolf-Hirschhorn syndrome candidate gene (midline fusion defect)	3	+
	Gpc1	Receptor	Albright hereditary osteodystrophy (AHO)–like syndrome candidate gene (obesity, brachydactyly, and ectopic ossifications)	3	+
Degenerative disease	*Rlbp1*	Signaling	Retinitis pigmentosa (retinal degeneration)	4	NC
	Aaas	Nuclear pore	Triple A syndrome (adrenal insufficiency, alacrima, achalasia)	2x pools	NC
	Ift57/Hippi	Signaling	Bardet-Biedl type 3 syndrome candidate gene (renal failure)	3	+
Cancer	*Smo*	Signaling	Gorlin's syndrome (basal cell carcinoma, medulloblastoma, rhabdomyosarcoma)	4	NC
	Prkar1a	Kinase	Carney complex, type 1 (myxomas of the heart and skin, endocrine tumors, lentiginosis)	4	+
	Stk11/Lkb1	Kinase	Peutz-Jeghers syndrome (pancreatic cancer, melanoma, testicular cancer, endocrine tumors; lentiginosis)	3	+

Sci Signal. Author manuscript; available in PMC 2013 October 04.